Inorganic Chemistry
Article

Inorg. Chem. **2010**, *49*, 5859–5867 **5859**
DOI: 10.1021/ic1000039

Preparation and Tunable Photoluminescence of Carbogenic Nanoparticles Confined in a Microporous Magnesium-Aluminophosphate

Yang Xiu,[†,‡] Qian Gao,[†,‡] Guo-Dong Li,[‡] Kai-Xue Wang,[†] and Jie-Sheng Chen*[,†]

[†]*School of Chemistry and Chemical Engineering, Shanghai Jiao Tong University, Shanghai 200240, P. R. China, and* [‡]*State Key Laboratory of Inorganic Synthesis and Preparative Chemistry, College of Chemistry, Jilin University, Changchun 130012, P. R. China*

Received January 1, 2010

Highly photoluminescent carbogenic nanoparticles (CNPs) have been prepared in MAPO-44, a Mg-substituted aluminophosphate molecular sieve with a chabazite structure, through thermal decomposition of the occluded template or loaded organic molecules. The resulting composite phosphors can be excited by a broad range of light in the ultraviolet region, and the emission wavelength is tunable through varying the thermal treatment condition. It is demonstrated that the emission wavelength is dependent on the carbon content in the composite phosphor materials, and the higher the content, the longer the emission wavelength. Correspondingly, upon excitation at a single UV wavelength, the emission color is finely tuned from violet to orange-red for samples with various carbon contents. X-ray photoelectron spectroscopy (XPS) and electron spin resonance (ESR) spectroscopy have been employed to elucidate the nature of the carbonaceous species in the phosphors. Heterogeneity or defects have been found to be prevalent in the CNPs of the composite phosphor materials, and it is these defects that form surface states responsible for the photoluminescence of the materials.

Introduction

Phosphors are a class of luminescent materials which find applications in a variety of fields. For example, daily lighting, projection televisions, fluorescent tubes, industrial tunable lasers, and X-ray intensifying screens all involve phosphors.[1−4] However, the commercially available phosphors are usually composed of costly or toxic metals (or metal activators), such as germanium, cadmium, or rare-earth elements.[3,5] Therefore, phosphor materials which are stable, efficient, and environmentally benign have attracted much attention recently.[6−12] Especially, with the emergence of violet light-emitting devices and lasers,[13] new phosphors that can be excited in the longer-wavelength UV range (340−400 nm) and have luminescence in the visible region may be used to manufacture fluorescent lamps without involving mercury. Among the new phosphors free of metal activators, the siloxane-based organic−inorganic hybrid materials[6−9] have been investigated extensively. For instance, Green et al.[6] prepared a series of highly emissive phosphors from alkoxysilane precursors, such as tetramethoxysilane or 3-aminopropyltriethoxysilane (APTES), and various carboxylic acids through a sol−gel route. In particular, the APTES−formic acid hybrid shows a photoluminescence efficiency (quantum yield 35 ± 1%) distinctly higher than those of the other luminescent materials[7−9] free of metal activators. Previously,

*To whom correspondence should be addressed. Fax: (+86)-21-54741297. E-mail: chemcj@sjtu.edu.cn.

(1) Blasse, G. *Chem. Mater.* **1989**, *1*, 294.
(2) Blasse, G.; Grabmaier, B. C. *Luminescent Materials*; Springer-Verlag: Berlin, 1994.
(3) Jüstel, T.; Nikol, H.; Ronda, C. *Angew. Chem., Int. Ed.* **1998**, *37*, 3084.
(4) Höppe, H. A. *Angew. Chem., Int. Ed.* **2009**, *48*, 2.
(5) Ropp, R. C. *Luminescence and the Solid State*; Elsevier: Amsterdam, Netherlands, 1991; Vol. *12*, pp 283−352.
(6) Green, W. H.; Le, K. P.; Grey, J.; Au, T. T.; Sailor, M. J. *Science* **1997**, *276*, 1826.
(7) (a) Brankova, T.; Bekiari, V.; Lianos, P. *Chem. Mater.* **2003**, *15*, 1855. (b) Bekiari, V.; Lianos, P. *Chem. Mater.* **1998**, *10*, 3777. (c) Bekiari, V.; Lianos, P. *Langmuir* **1998**, *14*, 3459.
(8) (a) Nunes, S. C.; de Zea Bermudez, V.; Cybinska, J.; Sá Ferreira, R. A.; Legendziewicz, J.; Carlos, L. D.; Silva, M. M.; Smith, M. J.; Ostrovskii, D.; Rocha, J. *J. Mater. Chem.* **2005**, *15*, 3876. (b) Fu, L.; Sá Ferreira, R. A.; Silva, N. J. O.; Carlos, L. D.; de Zea Bermudez, V.; Rocha, J. *Chem. Mater.* **2004**, *16*, 1507. (c) Carlos, L. D.; Sá Ferreira, R. A.; Pereira, R. N.; Assuno, M.; de Zea Bermudez, V. *J. Phys. Chem. B* **2004**, *108*, 14924. (d) Carlos, L. D.; Sá Ferreira, R. A.; de Zea Bermudez, V.; Ribeiro, S. J. L. *Adv. Funct. Mater.* **2001**, *11*, 111. (e) Carlos, L. D.; de Zea Bermudez, V.; Sá Ferreira, R. A.; Marques, L.; Assuno, M. *Chem. Mater.* **1999**, *11*, 581.
(9) Hayakawa, T.; Hiramitsu, A.; Nogami, M. *Appl. Phys. Lett.* **2003**, *82*, 2975.
(10) (a) Zhang, C.; Lian, H.; Kong, D.; Huang, S.; Lin, J. *J. Phys. Chem. C* **2009**, *113*, 1580. (b) Zhang, C.; Lin, C.; Li, C.; Quan, Z.; Liu, X.; Lin, J. *J. Phys. Chem. C* **2008**, *112*, 2183. (c) Lin, C. K.; Luo, Y.; You, H.; Quan, Z.; Zhang, J.; Fang, J.; Lin, J. *Chem. Mater.* **2006**, *18*, 458.
(11) (a) Feng, P. *Chem. Commun.* **2001**, 1668. (b) Zheng, N.; Bu, X.; Wang, B.; Feng, P. *Science* **2002**, *298*, 2366.
(12) Liao, Y. C.; Lin, C. H.; Wang, S. L. *J. Am. Chem. Soc.* **2005**, *127*, 9986.
(13) Narukawa, Y.; Kawakami, Y.; Fujita, S.; Fujita, S. *Phys. Rev. B* **1997**, *55*, 1938.

Published on Web 06/08/2010

we reported the preparation of highly photoluminescent activator-free ZnO nanocrystals (quantum yield about 45%) through a surface modification approach.[14]

Luminescent carbogenic nanoparticles (CNPs) are a new type of carbonaceous material which emit in the visible region under irradiation with UV light. In some sense, luminescent CNPs are advantageous over the conventional phosphors as they are chemically inert, biocompatible, and environmentally benign. Various techniques have been employed for the preparation of luminescent CNPs.[15−24] For instance, Liu et al.[15] reported the preparation of luminescent CNPs from candle soot through oxidative acid treatment, and the resulting CNPs with different emission colors were isolated through electrophoretic separation. Sun and co-workers[16,17] developed a laser ablation technique to prepare the CNPs from a carbon target followed by surface passivation with diamine-terminated oligomeric PEG_{1500N}, whereas Hu et al.[18] employed an improved one-step approach for the synthesis of luminescent CNPs though laser irradiation of a suspension of carbon materials in organic solvents. More recently, luminescent carbogenic dots were obtained by Peng and Travas-Sejdic[20] via surface passivation in an aqueous solution using carbohydrates as the starting materials. Nevertheless, the above-mentioned approaches for CNP preparation are usually sophisticated, and the obtained CNPs always require surface stabilization with organic (polymer) molecules to become luminescent[16−20] and dispersion in liquid to avoid agglomeration. These requirements inevitably affect the thermal stability of the resulting luminescent materials, limiting their practical applications to a considerable extent.

Aluminophosphate-based molecular sieves are microporous crystalline solids with widespread applications in areas such as catalysis and gas separation.[25−27] Well-defined synthesis conditions allow these molecular sieve materials to be highly transparent in the UV and visible regions, and in principle, their spatial confinement offers the advantage of formation of nanoparticles with photoluminescent properties. However, practical applications of aluminophosphate-based molecular sieves as host materials for accommodation of luminescent guest species have not been very successful, and the previously reported luminescent porous compounds are usually generated either by incorporating organic dyes or by doping with metal activators in the porous hosts.[28−30] Activator-free (or dye-free) microporous systems with tunable photoluminescence have not been achieved yet prior to our work.

In this article, we describe the preparation and characterization of a new type of stable, wavelength-tunable, and activator-free luminescent material, that is, host−guest phosphor systems with carbogenic nanoparticles confined in a Mg-substituted microporous aluminophosphate (MgAPO-44) solid. Upon excitation at a single wavelength, emissions with various wavelengths are obtained from the composite phosphors depending on the carbon content, which can be readily regulated through adjusting the preparation conditions. MgAPO-44, a magnesium-substituted aluminophosphate molecular sieve with a chabazite (CHA) structure (designated MAPO-CHA), has elongated cages (0.9×0.7 nm) interconnected through eight-member ring windows (0.4×0.4 nm). The CNPs located in the pores of the MAPO-CHA host are derived from the decomposition of the template reagent or the loaded small organic molecules without the need for further surface passivation, and the formation of the CNPs does not rely on sophisticated equipment such as a laser ablation apparatus.[16−18] In addition, the micropores of the MAPO-CHA host lattice offer a favorable microscopic environment for the facile regulation and stabilization of the ultrafine CNPs.

Experimental Section

Materials. Aluminum hydroxide was purchased from Aldrich. Absolute ethanol, acetone, glacial acetic acid, orthophosphoric acid (85 wt %), hydrofluoric acid (40 wt %), and hydrochloric acid (38 wt %) were all purchased from Beijing Chemical Factory; magnesium acetate ($Mg(CH_3COO)_2 \cdot 4H_2O$) and *n*-hexane were acquired from Tianjin No. 1 Chemical Reagent Factory, whereas cyclohexylamine was acquired from Shanghai Chemical Reagent Factory. All the reagents were of analytical grade and used as received without further purification. Deionized water (PURELAB Plus, PALL) was used in all of the experiments.

Sample Preparation. A. Synthesis of MAPO-CHA. The MAPO-CHA compound was synthesized from a hydrothermal reaction system by following the procedure described as follows. Under continuous stirring, 2.345 g (30.06 mmol) of $Al(OH)_3$ and 1.756 g (8.19 mmol) of $Mg(CH_3COO)_2 \cdot 4H_2O$ were dispersed in 20 mL of water, followed by the successive addition of 6 mL (42.5 wt %, aqueous solution, 32.76 mmol) of phosphoric acid, 3.62 mL (31.94 mmol) of cyclohexylamine and 1.5 mL (20 wt %, aqueous solution, 2 mmol) of hydrofluoric acid. The cyclohexylamine and the HF acid functioned as a template and a mineralizer, respectively. The gel mixture was stirred vigorously until becoming homogeneous and was sealed in a 50 mL PTFE-lined stainless steel autoclave, which was subsequently heated at 180 °C for 48 h under autogenous pressure. Afterward, the reaction system was slowly cooled to room temperature (RT). The resulting solid product was recovered by filtration, washed thoroughly with deionized water, sonicated to remove all the residual reagents or the loosely attached crystals, and dried at

(14) (a) Liu, D. P.; Li, G. D.; Su, Y.; Chen, J. S. *Angew. Chem., Int. Ed.* **2006**, *45*, 7370. (b) Liu, D. P.; Li, G. D.; Li, J. X.; Li, X. H.; Chen, J. S. *Chem. Commun.* **2007**, 4131.
(15) Liu, H.; Ye, T.; Mao, C. *Angew. Chem., Int. Ed.* **2007**, *46*, 6473.
(16) Sun, Y. P.; Zhou, B.; Lin, Y.; Wang, W.; Fernando, K. A. S.; Pathak, P.; Meziani, M. J.; Harruff, B. A.; Wang, X.; Wang, H.; Luo, P. G.; Yang, H.; Kose, M. E.; Chen, B.; Veca, L. M.; Xie, S. Y. *J. Am. Chem. Soc.* **2006**, *128*, 7756.
(17) Cao, L.; Wang, X.; Meziani, M. J.; Lu, F.; Wang, H.; Luo, P. G.; Lin, Y.; Harruff, B. A.; Veca, L. M.; Murray, D.; Xie, S. Y.; Sun, Y. P. *J. Am. Chem. Soc.* **2007**, *129*, 11318.
(18) Hu, S. L.; Niu, K. Y.; Sun, J.; Yang, J.; Zhao, N. Q.; Du, X. W. *J. Mater. Chem.* **2009**, *19*, 484.
(19) Liu, R.; Wu, D.; Liu, S.; Koynov, K.; Knoll, W.; Li, Q. *Angew. Chem., Int. Ed.* **2009**, *48*, 4598.
(20) Peng, H.; Travas-Sejdic, J. *Chem. Mater.* **2009**, *21*, 5563.
(21) Ray, S. C.; Saha, A.; Jana, N. R.; Sarkar, R. *J. Phys. Chem. C* **2009**, *113*, 18546.
(22) Bourlinos, A. B.; Stassinopoulos, A.; Anglos, D.; Zboril, R.; Georgakilas, V.; Giannelis, E. P. *Chem. Mater.* **2008**, *20*, 4539.
(23) (a) Lu, J.; Yang, J.; Wang, J.; Lim, A.; Wang, S.; Loh, K. P. *ACS Nano* **2009**, *3*, 2367. (b) Zhao, Q. L.; Zhang, Z. L.; Huang, B. H.; Peng, J.; Zhang, M.; Pang, D. W. *Chem. Commun.* **2008**, 5116.
(24) Zheng, L.; Chi, Y.; Dong, Y.; Lin, J.; Wang, B. *J. Am. Chem. Soc.* **2009**, *131*, 4564.
(25) Tian, Y.; Li, G. D.; Chen, J. S. *J. Am. Chem. Soc.* **2003**, *125*, 6622.
(26) Thomas, J. M. *Angew. Chem., Int. Ed.* **1999**, *38*, 3589.
(27) Davis, M. E. *Nature* **2002**, *417*, 813.
(28) Jüstel, T.; Wiechert, D. U.; Lau, C.; Sendor, D.; Kynast, U. *Adv. Funct. Mater.* **2001**, *11*, 105.
(29) (a) Chen, W.; Sammynaiken, R.; Huang, Y. *J. Appl. Phys.* **2000**, *88*, 1424. (b) Chen, W.; Sammynaiken, R.; Huang, Y. *J. Appl. Phys.* **2000**, *88*, 5188.
(30) Wada, Y.; Sato, M.; Tsukahara, Y. *Angew. Chem., Int. Ed.* **2006**, *45*, 1925.

ambient temperature. The dry sample was designated as-synthesized MAPO-CHA.

B. Preparation of Fully Carbonized MAPO-CHA (FC-MAPO). The as-synthesized MAPO-CHA was placed into a programmable tube furnace and heated from RT to 400 °C at a temperature ramp rate of 2 °C min^{-1} under an atmosphere of nitrogen. The system was kept at 400 °C for 3 h, followed by further heating to 550 °C at a rate of 1 °C min^{-1} and a 4-h isothermal hold at this temperature. The carbonization of the template was accomplished in this process, resulting in the fully carbonized MAPO-CHA (designated FC-MAPO) with a black color.

C. Preparation of Luminescent MAPO-CHA (C-MAPO). Under an atmosphere of oxygen with a flow rate of 0.5 L min^{-1}, the FC-MAPO was heated in the programmable tube furnace from RT to 550 at 4 °C min^{-1}, followed by a 2-h isothermal hold at 550 °C. The resulting carbon-containing sample was designated C-MAPO-A. For C-MAPO-B, -C, -D, and -E, the isothermal times in the heating process were controlled to be 30 min, 15 min, 10 min, and 5 min, whereas for C-MAPO-F the time was 5 min but the heating temperature was varied to 500 °C.

D. Preparation of Fully Detemplated MAPO-CHA (FD-MAPO). FD-MAPO was prepared in the same manner as that of C-MAPO-A, except that the isothermal temperature and time were 600 °C and 12 h, respectively. Snow-white crystals were obtained after this treatment.

E. Preparation of Luminescent MAPO-CHA from Loaded Organic Molecules. In a typical preparation, the FD-MAPO sample was submerged in acetone for 4 h, and the obtained solid with loaded acetone was then heated to 500 °C in a rate of 4 °C min^{-1} in the air, followed by a 20 min isothermal hold. The resulting solid product was designated AT-MAPO. Ethanol and acetic acid loaded samples were prepared similarly (the calcination temperature was 550 °C instead of 500 °C in this case), and the obtained products were designated ET-MAPO and AC-MAPO, respectively. The *n*-hexane−MAPO sample was obtained by the thermal treatment of *n*-hexane loaded FC-MAPO in a rapidly flowing atmosphere of N_2. The heating procedure was the same as that for AT-MAPO.

Characterization. The powder X-ray diffraction (XRD) patterns were recorded on a Rigaku D/Max 2550 X-ray diffractometer using Cu Kα radiation (λ = 1.5418 Å) over the 2θ range of 5−40° at room temperature. A JEOL JSM-6700F scanning electron microscope equipped with a standard secondary electron detector was used to image the inner cross-section of the crystals, which were dehydrated and embedded in conductive adhesive on the coppery specimen stage. Energy dispersive spectroscopy (EDS) was conducted to confirm the presence of carbon in the C-MAPO phosphors using an attached X-ray energy dispersive spectroscopy system, whereas the carbon contents of the bulk samples were determined through elemental analysis on a Perkin-Elmer 2400 elemental analyzer. The infrared spectra were obtained with a Bruker IFS 66 V/S FTIR spectrometer using KBr pellets, and the Raman spectra were recorded at ambient temperature on a Jobin-Yvon T64000 spectrometer with an excitation wavelength of 514.5 nm. The TEM images were taken on a JEOL JEM-3010 transmission electron microscope operating at an accelerating voltage of 300 kV. N_2 adsorption/desorption measurements were performed on a Micromeritics ASAP 2020 M instrument after the samples were degassed at 200 °C and 1×10^{-5} Torr for 10 h prior to the measurements. A Perkin-Elmer LS 55 luminescence spectrometer was used to obtain the excitation and emission spectra for all of the solid products. The X-ray photoelectron spectra (XPS) were recorded on a VG ESCALAB MK II electron spectrometer, whereas the electron spin resonance (ESR) spectroscopy was performed on a JEOL JES-FA200 spectrometer operating in the X-band mode. The *g* values were calculated by comparison with the spectrum of 1,1-diphenyl-2-picrylhydrazyl (DPPH), whereas the spin concentrations were determined by comparing the recorded spectra with that of a Mn marker and DPPH, using the built-in software of the spectrometer.

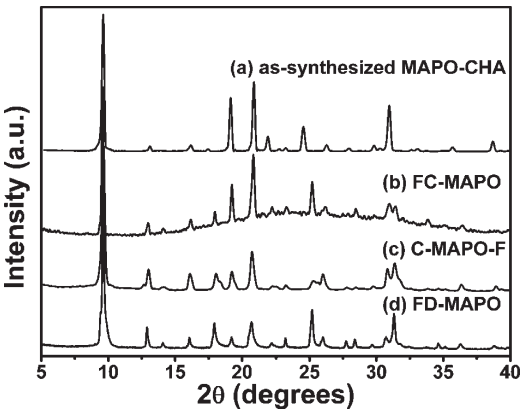

Figure 1. Powder X-ray diffraction patterns of as-synthesized MAPO-CHA (a), FC-MAPO (b), C-MAPO-F (c), and FD-MAPO (d).

Results and Discussion

General Characterization. Figure 1 shows the XRD patterns of the as-synthesized MAPO-CHA (a), FC-MAPO (b), C-MAPO-F (c), and FD-MAPO (d). These samples show characteristic diffraction peaks which are in good agreement with the standard data of MAPO-CHA with and without template molecules.[31] In the pattern of FC-MAPO, a broad peak ranging from 12° to 36° (the so-called graphite peak) is observed, indicative of the presence of a graphite-like structure of carbon. This observation suggests that the template cyclohexylamine is decomposed by the thermal treatment in the N_2 atmosphere, and the resulting carbon fragments are accumulated in the host lattice of the MAPO-CHA material. The broad peak disappears for the C-MAPO-F derived from oxidation of FC-MAPO because the amount of the carbonaceous matter in this sample is too low to be detected by XRD. However, the energy dispersive spectroscopy (EDS) analysis (Figure 2) conducted on the inner cross-section of the crystals confirms the presence of carbon atoms, although in a very small amount, in the partly oxidized sample C-MAPO-F. The disappearance of the broad carbon peak in the XRD pattern of C-MAPO-F indicates that the oxidation process can regulate the carbon content in the microporous host material. From Figure 1 it is also seen that the thermal treatment does not affect the crystalline structure of the MAPO material, as the main diffraction peaks remain after the thermal treatment for both C-MAPO-F and FD-MAPO (the variation in relative peak intensity and position arises from the removal of the template molecules after detemplating), and no new crystalline phases appear in the final product.

The as-synthesized MAPO-CHA, the FC-MAPO, and the C-MAPO-F samples are further characterized through FTIR spectroscopy. In the FTIR spectrum of the as-synthesized MAPO-CHA (Figure 3Aa), there appear bands at 1454 cm^{-1}, 1508 cm^{-1}, and 1606 cm^{-1} which are associated with the methylene symmetric bending

(31) Lohse, U.; Parlitz, B.; Müller, D.; Schreier, E.; Bertram, R.; Fricke, R. *Microporous. Mater.* **1997**, *12*, 39.

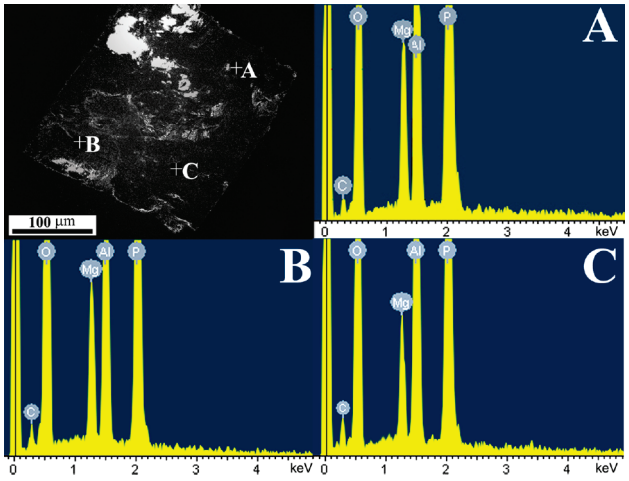

Figure 2. Energy dispersive spectrum of the inner cross-section of a C-MAPO-F crystal. The carbon signals with an essentially identical intensity are present at sites A, B, and C, indicating that the carbogenic species were distributed homogeneously in the crystal.

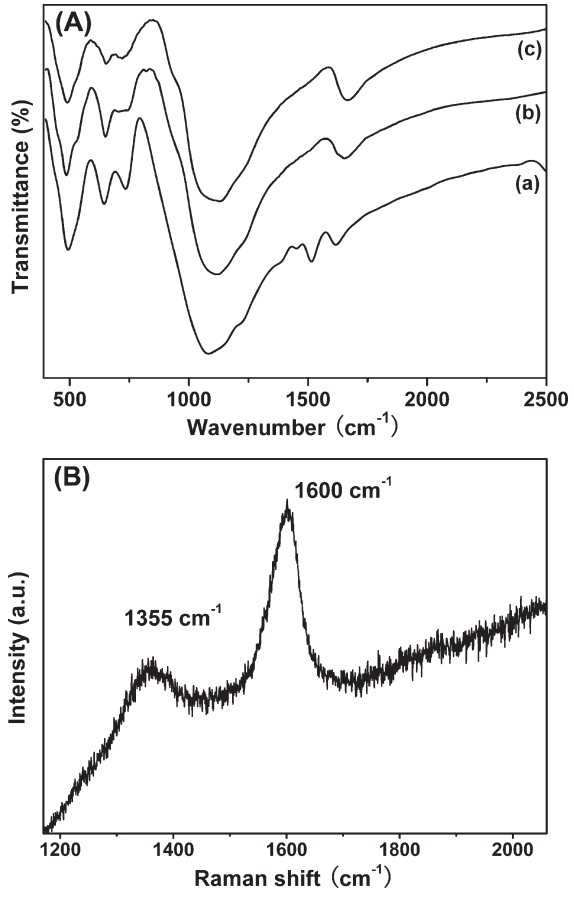

Figure 3. FTIR spectra (A) of as-synthesized MAPO-CHA (a), FC-MAPO (b), and C-MAPO-F (c) and Raman spectrum (B) of FC-MAPO.

vibrations, C−N stretching vibrations, and N−H bending vibrations of the template molecules, respectively. All the other bands are assignable to the framework vibrations of the chabazite structure, such as the O−P−O asymmetric stretching vibration in PO_4 groups (1081 cm^{-1}), the P−O−Al asymmetric stretching vibration

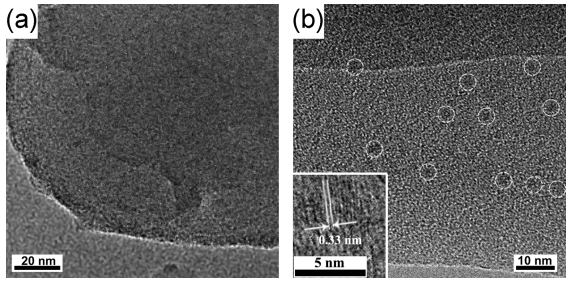

Figure 4. TEM images of C-MAPO-E (a) and carbogenic nanoparticles (b) obtained by removing the host lattice of C-MAPO-E with concentrated hydrochloric acid. Inset is the HRTEM image of a typical CNP.

(1213 cm^{-1}), and T−O bending vibration for the double-6-rings (644 cm^{-1}).[32] In Figure 3Ab and Ac, the characteristic framework vibrations which are also present in Figure 3Aa are observed, but the template bands disappear for FC-MAPO and C-MAPO-F, confirming that the thermal treatment leads to template decomposition with the framework integrity of the MAPO material being maintained.

Although the attempt to obtain the Raman spectra of the oxidized samples (the C-MAPO materials) was not successful due to their intense photoluminescent emissions, the Raman spectrum of FC-MAPO, which was used as the precursor for the formation of the C-MAPO composite phosphors, has been recorded (Figure 3B). Two peaks centered at 1600 cm^{-1} and 1355 cm^{-1} appear in the Raman spectrum with the former being attributable to graphite-like carbon with an sp^2 configuration.[33a] The slight deviation of this 1600 cm^{-1} peak from that (1580 cm^{-1}) for ideal crystalline graphite indicates that the size of the graphite-like carbon in FC-MAPO is in the nanometer range.[33b,c] The 1355 cm^{-1} band is associated with the breathing mode of A_{1g} symmetry.[33b] Because this vibrational mode is forbidden in ideal graphite and only observable in an imperfect graphite structure, disordered or defective regions are considered to be present in the carbon matter of the FC-MAPO sample.

Figure 4a shows the TEM image of the C-MAPO-E material collected on a carbon grid. Owing to the low contrast, the CNPs in this sample are not observed in the TEM micrograph. However, if the MAPO host lattice is removed with concentrated hydrochloric acid, CNPs can be isolated through centrifugation of the acid-treated product. As shown in Figure 4b and Figure S1 (Supporting Information), the isolated CNPs are spherical with a uniform size (ca. 4 nm). In principle, the size of the carbogenic nanoparticles confined in the micropores should not exceed the cage size of the inorganic MAPO host. Therefore, the significant difference between the size of the isolated CNPs (4 nm) and the diameter (0.9 nm) of the CHA micropores indicates that the isolated CNPs are formed through agglomeration of the primary carbogenic particles initially occluded in the C-MAPO-E host. Particle agglomeration is very common for ultrafine powders and nanoparticles, but within the host lattice

(32) van Heyden, H.; Mintova, S.; Bein, T. *Chem. Mater.* **2008**, *20*, 2956.

(33) (a) Ferrari, A. C.; Robertson, J. *Phys. Rev. B* **2001**, *64*, 075414. (b) Ferrari, A. C.; Robertson, J. *Phys. Rev. B* **2000**, *61*, 14095. (c) Ferrari, A. C.; Meyer, J. C.; Scardaci, V.; Casiraghi, C.; Lazzeri, M.; Mauri, F.; Piscanec, S.; Jiang, D.; Novoselov, K. S.; Roth, S.; Geim, A. K. *Phys. Rev. Lett.* **2006**, *97*, 187401.

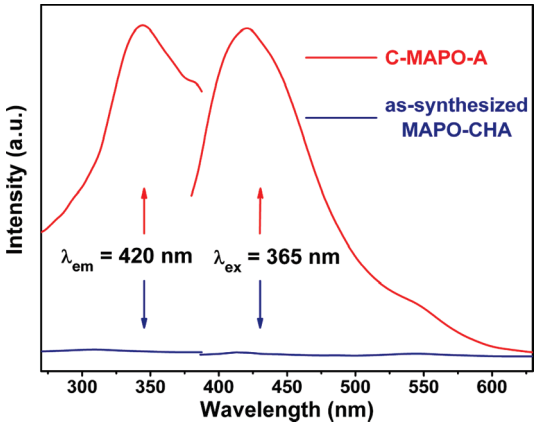

Figure 5. Emission and excitation spectra of as-synthesized MAPO-CHA (blue line) and C-MAPO-A (red line). The emission spectra were recorded at 365 nm excitation, whereas the excitation spectra were acquired with a detection wavelength of 420 nm.

of the microporous MAPO, the ultrafine CNPs are well-protected and are prevented from agglomeration. The inset of Figure 4b illustrates a lattice spacing of 0.33 nm, which is very close to the graphite 002 lattice spacing.[22] After isolation from the MAPO host, the CNPs can be easily dispersed in ethanol, acetone, and acidic or alkaline aqueous solutions, and these dispersion systems remain stable for at least one month without precipitation. To clarify whether the confined CNPs affect the microporosity of the host materials, N_2 adsorption/desorption measurements for the FD-MAPO and the C-MAPO-E samples have been performed. The surface area based on the BET model for FD-MAPO is calculated to be 642 cm^2/g, whereas that for C-MAPO-E is 529 cm^2/g. The pore size for both samples is approximately 0.5 nm (Figure S2, Supporting Information). The small differences in BET surface area and pore size distribution of the MAPO materials with and without CNPs indicate that the presence of CNPs in the C-MAPO samples does not affect the adsorption property of the host materials significantly.

Photoluminescent Properties. Figure 5 shows the excitation and emission spectra for the as-synthesized MAPO-CHA and the C-MAPO-A samples at ambient temperature. No peaks are observed for the excitation and emission spectra of the as-synthesized MAPO-CHA. In contrast, the C-MAPO-A material shows strong excitation and emission peaks. Upon irradiation with UV light (365 nm), the C-MAPO-A sample exhibits a broad emission centered at about 420 nm, and correspondingly a violet color appears to the naked eye for the sample. The excitation spectrum of C-MAPO-A consists of a broad band with a maximum at 344 nm, suggesting that the sample can be excited by the light over a broad range in the ultraviolet region. This observation demonstrates that, through simple thermal treatment, the nonluminous MAPO-CHA precursor can be made highly photoluminescent at ambient temperature. On the other hand, it is noted that the fully detemplated FD-MAPO sample is not luminous either, suggesting that the CNPs occluded in the C-MAPO materials are responsible for the photoluminescence of the phosphors.

The luminescent property of the C-MAPO phosphors depends on the oxidative pyrolysis condition. As shown in Figure 6, all six representative samples obtained under different conditions exhibit photoluminescence at room temperature upon excitation at 365 nm. The recorded PL spectra show that the emission peak of C-MAPO-A to -F varies from 420 to 550 nm. Correspondingly, the observed emission color changes from violet through blue, cyan, green, and yellow to orange-red. It is obvious that the emission wavelength is dependent on the isothermal time. Specifically, a longer time of oxidative pyrolysis leads to a shorter wavelength for the C-MAPO emission. In order to reveal the reason behind this observation, elemental analysis of the C-MAPO samples has been performed, and the analysis result shows that the carbon contents in C-MAPO-A, -C, and -F are 0.24, 0.39, and 1.20 wt %, respectively (Table S1, Supporting Information). These data demonstrate that the amount of carbon in the C-MAPO material is inversely proportional to the isothermal time. In addition, the isothermal temperature for C-MAPO-F is 500 °C, lower than that (550 °C) for other C-MAPO samples, and as a result, the carbon content in this sample is distinctly higher. On the basis of the analysis result, it is concluded that the PL wavelength of the C-MAPO material is correlated with the carbon content in the material. Consequently, through varying the oxidative pyrolysis condition and hence the carbon content, C-MAPO phosphors with tunable emission colors, from violet to orange-red, can be easily obtained.

To further confirm the contribution of CNPs to the PL property of C-MAPO phosphors, FD-MAPO, AT-MAPO, ET-MAPO, and AC-MAPO samples have been prepared (see the Experimental Section) for comparison. In this preparation, the fully detemplated material FD-MAPO, which contains no carbonaceous matter at all, is infused with acetone (AT), ethanol (ET), and acetic acid (AC), respectively, followed by oxidative pyrolysis in the air. The recorded PL spectra for these samples are shown in Figure 7. It is seen that no photoluminescence is exhibited by the FD-MAPO material (Figure 7a), indicating that the MAPO host is completely nonluminous. In contrast, the AT-MAPO, AC-MAPO, and ET-MAPO samples emit intense light upon excitation (Figure 7a,b). This observation demonstrates that the photoluminescent property of the MAPO material can be conferred upon through generation of carbogenic species in the pores of the material. Figure 7b shows the PL spectra of AT-MAPO phosphors prepared at 500 °C with various isothermal times. It is seen that the emission wavelength decreases with increasing the isothermal time, in a manner similar to that for the C-MAPO phosphors prepared from the FC-MAPO precursor. Because acetone, ethanol, and acetic acid cannot be the direct emissive centers, the formation of CNPs from the carbonization of these guest molecules in the MAPO host is considered to be responsible for the photoluminescence. For the restriction of the micropores, a proportion of the infused organic molecules cannot volatize as the temperature is elevated rapidly, and they decompose into carbon fragments and accumulate within the micropores of FD-MAPO, resulting in the photoluminescent CNPs.

Our experiment indicates that CNP-containing MAPO materials with photoluminescent properties are able to be obtained either through direct oxidative pyrolysis of the FC-MAPO precursor or through organic loading

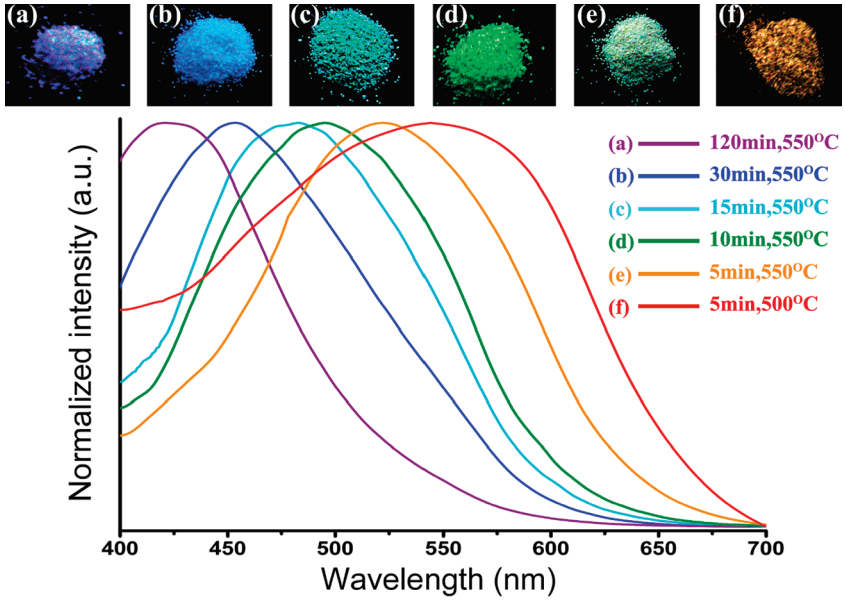

Figure 6. PL emission spectra and photographs of C-MAPO samples under UV irradiation: (a) C-MAPO-A, 120 min, 550 °C; (b) C-MAPO-B, 30 min, 550 °C; (c) C-MAPO-C, 15 min, 550 °C; (d) C-MAPO-D, 10 min, 550 °C; (e) C-MAPO-E, 5 min, 550 °C; and (f) C-MAPO-F, 5 min, 500 °C. For clarity, the PL intensities were normalized.

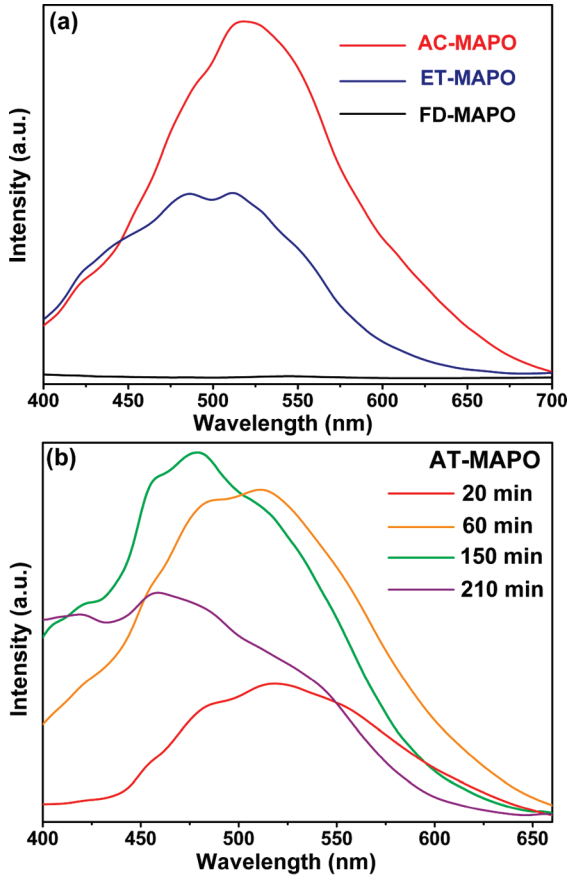

Figure 7. PL emission spectra (a) of AC-MAPO (red line), ET-MAPO (blue line), and FD-MAPO (black line) and PL emission spectra (b) of AT-MAPO prepared at 500 °C with an isothermal time of 20 min (red line), 60 min (orange line), 150 min (green line), and 210 min (violet line).

followed by thermal treatment. Unlike the photoluminescent CNP materials reported in the literature,[16−20] our materials do not need further passivation with polymers or other organic molecules for photoluminescence, and the thermal stability of our materials is obvious because they have been subjected to thermal treatment at elevated temperatures (at least 500 °C). In contrast, the polymer-passivated CNPs are inherently unstable toward thermal treatment because of the decomposition of polymer molecules at elevated temperatures (nonpassivated CNPs tend to agglomerate,[21] losing their luminescent property). Furthermore, we can tune the emission wavelength at a fixed excitation wavelength simply through varying the carbon contents in the C-MAPO materials, whereas the previously reported CNP materials usually need to use different excitation wavelengths to achieve different emission wavelengths.[16,17,19,20]

We have also estimated the external photoluminescent quantum yields of the materials we obtained through the Wrighton−Ginley−Morse method using magnesium oxide as a reflecting standard (for details, see the Supporting Information).[34] For C-MAPO-A to -F, the quantum yields are about 12, 26, 23, 19, 12, and 7%, respectively. These values are comparable with those for the reported siloxane-based phosphors in the solid state.[7c,8a,b,d] On the other hand, it is noted that the AC-MAPO shows an external quantum yield of ca. 40%, distinctly higher than those for the other samples. The high quantum yield in combination with the high thermal stability renders our materials promising for practical applications.

Origin of Photoluminescence for C-MAPO Materials. Since the microporous host material MAPO-CHA is not photoluminescent, the PL property of the composite C-MAPO phosphors must arise from the CNPs occluded in the host lattice. X-ray photoelectron spectroscopy (XPS) has been employed to characterize the CNPs in the C-MAPO samples. Figure 8 shows the C1s XPS spectra of FC-MAPO, C-MAPO-A, C-MAPO-E, and

(34) Wrighton, M. S.; Ginley, D. S.; Morse, D. L. *J. Phys. Chem.* **1974**, *78*, 2229.

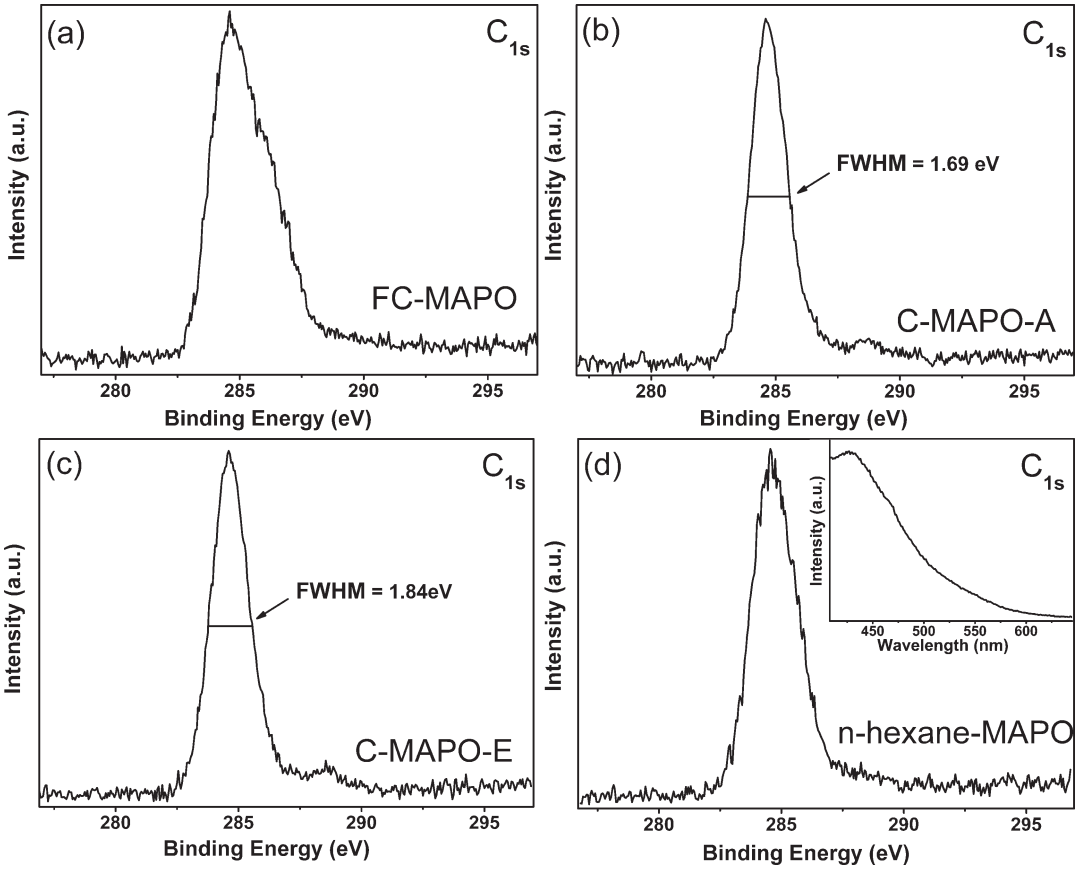

Figure 8. C_{1s} XPS spectra for FC-MAPO (a), C-MAPO-A (b), C-MAPO-E (c), and *n*-hexane-MAPO (d) with the corresponding PL spectrum in the inset.

n-hexane-MAPO. As is known, the C1s XPS spectrum of single crystalline graphite is dominated by an intense, asymmetric peak centered at 284.6 eV with a long tail at the higher binding energy side.[35,36] The main peak in the spectra (Figure 8a−d) for the carbon-containing samples is in accordance with that of graphite in the peak position (284.6 eV), and therefore this peak is attributable to graphite-like carbon atoms with sp^2 hybridization.[36] In the spectrum of FC-MAPO, there appears a unique shoulder at 285.9 eV, assignable to the C═N bonds[37,38] formed from decomposition of the template cyclohexylamine during the carbonization process. This shoulder peak is not observed in the photoluminescent C-MAPO samples, suggesting that oxidation of the FC-MAPO removes the C═N bonds in the carbon matter. On the other hand, in the spectra of C-MAPO-A and -E (Figure 8b,c), there appears a small peak at 288.5 eV besides the main peak. Peaks at this position (288.5 eV) are considered to arise from carbon atoms bound to oxygen atoms,[35] and therefore carbonyl (C═O) groups[39,40] are thought to be present in the C-MAPO-A and -E samples. Furthermore, it is noted that the full width at half-maximum (FWHM) of the main peak in C-MAPO-A and -E is 1.69 and 1.84 eV, distinctly larger than that for ideal graphite (0.35 eV).[41] Because the graphite peak FWHM depends on the heterogeneity (or defects) of the graphene layers in carbon matter (the more heterogeneous the graphene layers, the wider the graphite peak),[42,43] the C-MAPO samples should contain CNPs with a considerable amount of defects such as sp^3-hybridization carbon atoms, broken bonds, and heteroatoms.[43] These defects are believed to play a role in the photoluminescence of the C-MAPO materials.

Electron spin resonance spectroscopy (ESR) has been performed to reveal the relationship between the defects of CNPs and the PL property of the C-MAPO materials. As shown in Figure 9, no ESR signal is observed for the as-synthesized MAPO-CHA and the fully detemplated FD-MAPO samples, whereas the carbon-containing samples all exhibit distinct ESR signals. These ESR signals at $g = 2.003$, characteristic of free radicals, indicate the presence of paramagnetic centers in the C-MAPO phosphors. The line width for AC-MAPO is 0.64 mT, and that for C-MAPO-F is 0.58 mT. Because the MAPO molecular sieve host lacks magnetic components, the paramagnetic centers must be associated with the carbogenic species in the C-MAPO materials. As demonstrated by the XPS spectroscopy, there are many defects in the CNPs of

(35) Kovtyukhova, N. I.; Mallouk, T. E.; Pan, L.; Dickey, E. C. *J. Am. Chem. Soc.* **2003**, *125*, 9761.
(36) Ago, H.; Kugler, T.; Cacialli, F.; Salaneck, W. R.; Shaffer, M. S. P.; Windle, A. H.; Friend, R. H. *J. Phys. Chem. B* **1999**, *103*, 8116.
(37) Waltman, R. J.; Pacansky, J.; Bates, C. W. *Chem. Mater.* **1993**, *5*, 1799.
(38) Stankovich, S.; Piner, R. D.; Chen, X.; Wu, N.; Nguyen, S. B. T.; Ruoff, R. S. *J. Mater. Chem.* **2006**, *16*, 155.
(39) Eberhardt, W.; Sham, T. K.; Carr, R.; Krummacher, S.; Strongin, M.; Weng, S. L.; Wesner, D. *Phys. Rev. Lett.* **1983**, *50*, 1038.
(40) Su, C. Y.; Xu, Y.; Zhang, W.; Zhao, J.; Tang, X.; Tsai, C. H.; Li, L. J. *Chem. Mater.* **2009**, *21*, 5674.
(41) Watanabe, M. O.; Itoh, S.; Mizushima, K.; Sasaki, T. *Appl. Phys. Lett.* **1996**, *68*, 2962.
(42) Darmstadt, H.; Roy, C.; Kaliaguine, S.; Kim, T. W.; Ryoo, R. *Chem. Mater.* **2003**, *15*, 3300.
(43) Darmstadt, H.; Roy, C. *Carbon* **2003**, *41*, 2662.

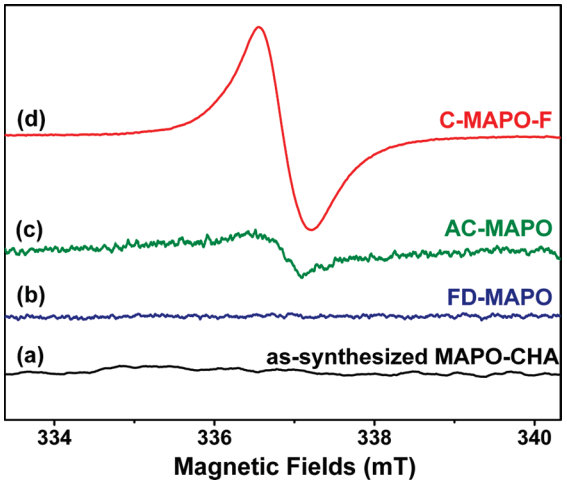

Figure 9. ESR spectra of as-synthesized MAPO-CHA (a), FD-MAPO (b), AC-MAPO (c), and C-MAPO-F (d).

C-MAPOs. These defects are believed to be responsible for the presence of localized radicals,[44,45] which give rise to the ESR signals in the samples. Figure 10a displays the relationship between the emission wavelength and the electron spin concentration calculated from the corresponding ESR spectra. It is seen that the emission wavelength is proportional to the spin concentration, which corresponds to the carbon content in the C-MAPO material. The higher the carbon content, the larger the spin amount, and therefore it is concluded that the emission wavelength of the C-MAPO phosphors is dependent on the carbon content in the materials.

It is presumed that the thermal treatment of the occluded template or loaded organic molecules in the micropores of the MAPO host leads to the formation of CNPs with defects, and these defect-containing CNPs are separated and protected by the MAPO host lattice. The defects result in electron localization,[46−48] and a certain amount of surface states are thus present to accommodate these localized electrons. Upon excitation by UV light, the CNPs with surface states are excited and the radiative relaxation of the excited CNPs releases energy in the form of emitted visible light, leading to photoluminescence. It is found that the emission intensity is correlated with the carbon content in the C-MAPO materials. With increase in carbon content from C-MAPO-A to C-MAPO-F, the emission intensity increases initially, followed by reaching a maximum for the sample C-MAPO-B and a subsequent decrease for the rest of the samples (Figure 10b). This observation is easily rationalized on the basis of competition between concentration contribution and the quenching of luminescent centers in the CNPs. As revealed by the ESR spectroscopy, the concentration of CNP defects which determines the amount of the surface states is proportional to the carbon content in the C-MAPO

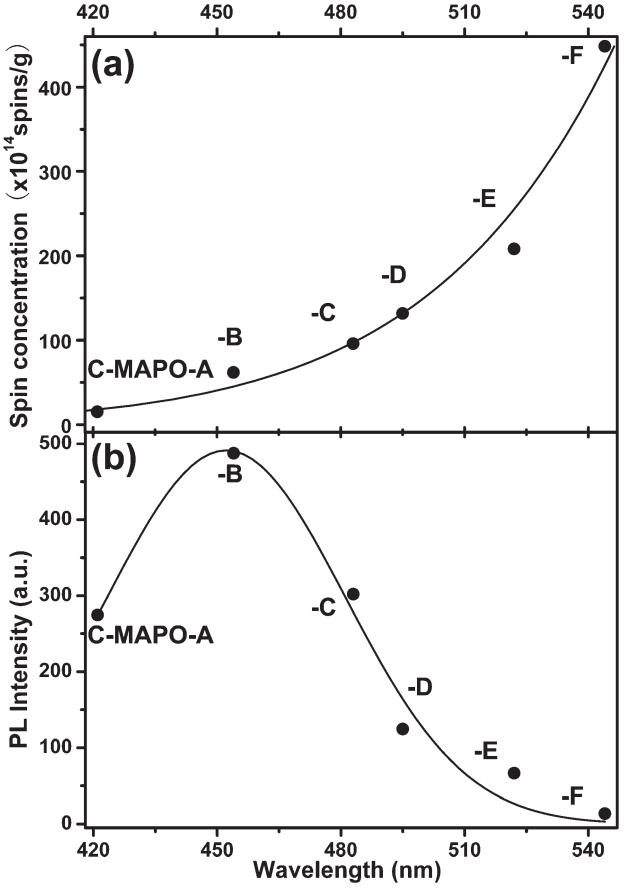

Figure 10. Plots of spin concentration (a) and PL intensity (b) versus emission wavelength for C-MAPO-A through -F.

materials. That is, the higher the carbon content, the more defects which act as luminescent centers. A higher concentration of luminescent centers contributes more to the emission intensity. But if the concentration is too high, concentration quenching of emission intensity would dominate as observed for conventional phosphors. Therefore, the samples (e.g., C-MAPO-F) with a distinctly high carbon content show weaker emissions than those with a moderate amount of carbon. The PL spectrum of FC-MAPO shows a very weak emission (Figure S3, Supporting Information). Its PL intensity is so low that the emission is not clearly observable by the naked eye under a UV lamp. Since FC-MAPO is formed from the decomposition of the template under a N_2 atmosphere, it has the highest carbon content among all of the C-MAPO samples. Therefore, the high carbon content is believed to result in a high concentration of luminescent centers which severely quench the photoluminescence.

To elucidate the effect of O-containing groups (such as C=O and C−OH) on photoluminescence, we prepared *n*-hexane-MAPO through thermal treatment of *n*-hexane-infused FD-MAPO under an atmosphere of N_2. No signal related with C=O (or C−OH) bonds except for an intense peak of graphite-like carbon centered at 284.6 eV with a weak shoulder at 285.2 eV assignable to carbon atoms with sp^3 hybridization is observed in the C1s XPS spectrum of the sample (Figure 8d). The *n*-hexane−MAPO material free of O-containing groups also emits visible light (inset of Figure 8d) under excitation at

(44) Menachem, C.; Wang, Y.; Flowers, J.; Peled, E.; Greenbaum, S. G. *J. Power Sources* **1998**, *76*, 180.
(45) Alcántara, R.; Ortiz, G. F.; Lavela, P.; Tirado, J. L.; Stoyanova, R.; Zhecheva, E. *Chem. Mater.* **2006**, *18*, 2293.
(46) Enoki, T.; Kobayashi, Y. *J. Mater. Chem.* **2005**, *15*, 3999.
(47) Tomita, S.; Sakurai, T.; Ohta, H.; Fujii, M.; Hayashi, S. *J. Chem. Phys.* **2001**, *114*, 7477.
(48) Goettmann, F.; Fischer, A.; Antonietti, M.; Thomas, A. *Angew. Chem., Int. Ed.* **2006**, *45*, 4467.

365 nm, suggesting that the presence of O-containing groups is not necessary for the photoluminescence of the C-MAPO materials. Nevertheless, the possibility that the C═O (or C−OH) groups help to enhance the photoluminescence of the CNPs is not excluded, as the AC-MAPO sample which contains a considerable amount of C═O (or C−OH) groups (the carbon content of AC-MAPO is 0.36 wt % (Table S1, Supporting Information), comparable with that of C-MAPO-C) exhibits the highest quantum yield among all of the samples.

Conclusions

CNP-loaded magnesium-aluminophosphate solid phosphors with tunable emission wavelength ranging from 420 to 550 nm have been prepared through thermal treatment of the host crystals under different conditions. It is revealed that the carbogenic species in the phosphors is responsible for the observed photoluminescence, and the emission wavelength depends on the carbon content in the materials. XPS and ESR spectroscopies demonstrate that the PL property arises from defects which render electron localization in the CNPs possible. Upon irradiation with UV light, the surface states with the localized electrons in the CNPs are excited, whereas the radiative relaxation of the excited surface states releases energy, emitting visible light. The emission intensity is also correlated with the carbon content in the phosphor materials. At a lower carbon content, the emission intensity increases with the content, whereas at a higher carbon content, the emission intensity is inversely proportional to the content because of the competition between concentration contribution and quenching of the luminescent centers in the phosphors. In contrast with the previously reported CNP phosphors which are coated with organic molecules, our phosphor materials possess high thermal stability since the materials have been subject to elevated temperatures during the preparation process. It is anticipated that the preparation approach we adopted may be extended to other solid CNP phosphors with high thermal stability and superior luminescent properties.

Acknowledgment. This work was supported by the National Natural Science Foundation of China (20731003) and the National Basic Research Program of China (2007CB613303).

Supporting Information Available: TEM images of CNPs isolated from C-MAPO-D, C-MAPO-F, and FC-MAPO; pore size distribution of FD-MAPO and C-MAPO-E; PL emission spectrum of FC-MAPO; results of C,H,N elemental analysis; and the detailed procedure for calculation of the quantum yields. This material is available free of charge via the Internet at http://pubs.acs.org.